Biophysical Journal, Volume 99

Supplemental Data

Title: The electrostatic origin of salt-induced nucleosome array compaction

Authors: Nikolay Korolev, Abdollah Allahverdi, Ye Yang, Yanping Fan, Alexander P Lyubartsev, and Lars Nordenskiöld

“The electrostatic origin of salt-induced nucleosome array compaction”

by Nikolay Korolev, Abdollah Allahverdi, Ye Yang, Yanping Fan, Alexander P. Lyubartsev, and Lars Nordenskiöld

Supporting Computational Methods

"Sphere-Bead" model of the NCP and chromatin array.

The Nucleosome Core Particle (NCP) model was described in our previously published work (see Supporting Material of ref. (1), http://www.biophysj.org/biophysj/supplemental/S0006-3495(09)00318-X).

A central neutral spherical particle of effective radius 3.5 nm represents the globular domain of the histone octamer (HO). The DNA wrapped around the core is modeled by 25 beads of effective radius 1.0 nm (Fig. S1). Each DNA bead models a 6 bp DNA fragment. The original −12e charge of each DNA bead is reduced to −9.44e assuming that the DNA phosphate groups contacting the NCP core are neutralized by positive charges of the histone octamer core, which for this reason carries no charge.

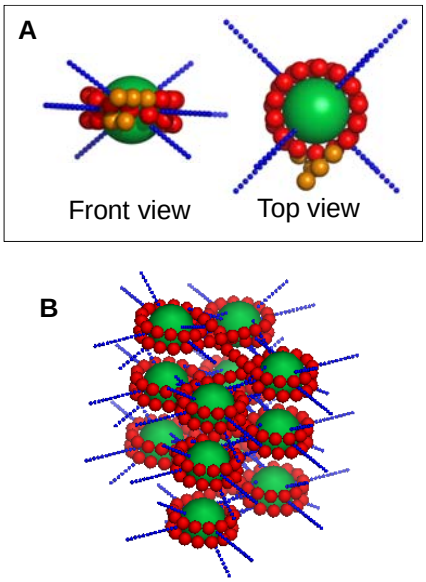

Fig. S1. (**A**). "Sphere-Bead" model of the nucleosome; partially neutralized DNA beads are red; fully charged beads modeling the linker DNA are orange. (**B**). Model of the "12-177" nucleosome array (initial configuration in the simulation cell).

Analysis of charge distribution in the NCP. To justify this assumption we carried out an analysis of the NCP atomic structure and made a number of test simulations with variations of the NCP models where a negative or positive charge of the central particles was applied. Below a brief summary of the analysis of charged amino acid distribution in the globular histone octamer core is given:

Counting charged amino acids in the histone core in the crystal structure PDB code 1KX5 (2) shows that the core histones carry a net charge +58e which is composed of the positive charges of 70 Arg and 52 Lys amino acids as well as negative charges of 20 Asp and 44 Glu amino acids (in the present model two short C-terminal tails of the H2A histones were merged to the central core particle). We analyzed the spatial distribution of the NZ and CZ

atoms of the respectively Lys and Arg amino acids relative to the phosphate groups of the DNA wrapped around the histone core and found that 30 Lys and 40 Arg residues make respectively 68 P-NZ and 128 P-CZ contacts with distances shorter than 1.0 nm. Detailed inspection of these contacts showed that most of these basic amino acids, 58 to 70 of them (depending on the definition of the cutoff and number of observed pairs) can be counted as residues neutralizing the charge on the DNA. Our analysis is in line with earlier observation (3) and recent analysis (4) that the basic amino acids are concentrated on the lateral surface of the histone core and direct the DNA wrapping. After subtracting the positive charge of the basic amino acids involved in neutralization of the DNA charge, the net charge of the histone core appears to be neutral or negative (up to −12e and depending on the choice of cutoff). Therefore, assigning a positive charge to the central particle representing the core domain of the histone octamer does not reflect the charge distribution of the real NCP. Instead, we use a neutral core and reduced the charge of the DNA wrapped on the core to account for the neutralizing contribution of the closely located basic amino acids.

There is an "acidic islet" (5, 6) on each of the surfaces of the NCP "cylinder" which is formed by a cluster of 5 Glu and Asp amino acids of the H2A histones (see Fig. S2 illustrating the distribution of the charged residues on the surface of the NCP where the acidic islet is highlighted). These acidic patches might play an important role in formation of ordered chromatin structures (7, 8). Within the present description of the HO core as a spherical particle, the effects of the acidic patch can be approximated by assigning a negative charge of −10e to it.

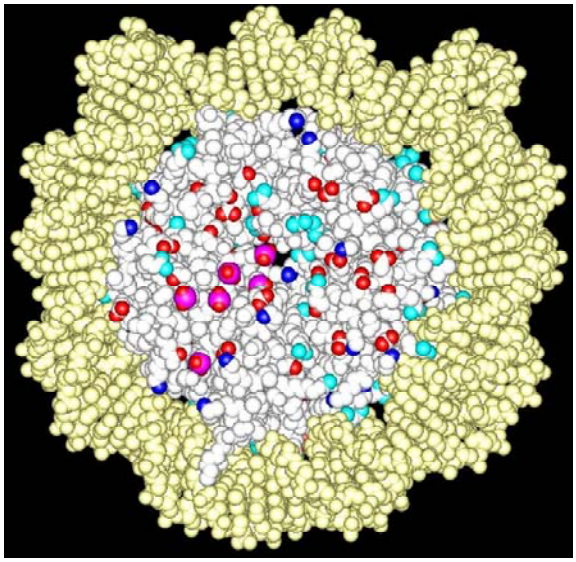

Fig. S2. Distribution of charged groups on the surface of the histone globular domain in the NCP crystal structure PDB code 1KX5 (2) presenting atoms as white (histone octamer) or yellow (DNA) van der Waals spheres. Nitrogen atoms of the Lys (NZ) and Arg (NH1,NH2) amino acids are drawn in blue and cyan respectively; oxygen atoms of the carboxylate groups of the Glu and Asp are in red; carbon atoms of the carboxylate groups comprising the "acidic islet" are shown in magenta.

We then made some estimates of the sensitivity of the simulations to the choice of the charge of the central particle testing two models with neutral or negatively charged (−10e) central particle (the charge of each of the DNA beads was changed accordingly to −9.44e or −9.04e). We found that the results obtained using these slightly different models are similar.

Simulations for the Mg-system at C_{Mg} = 1.58 mM (pre-folded state) resulted in values of $s_{20.w}$ and R_g of 38.3 and 23.1 as well as 38.6 and 22.9 for negative and neutral cores respectively. At 3.89 mM Mg^{2+} (folded state), these values of $s_{20.w}$ and R_g are 47.5±2.2 S and 16.0 ± 1.4 nm as well as 47.4±1.3 S and 16.5±0.7 nm for negative and neutral cores respectively. For $CoHex^{3+}$ at 1.055 mM (folded state), $s_{20.w}$ and R_g are equal to 56.3±0.8 S and 12.6±0.4 nm as well as 58.9±0.9 S and 12.0±0.3 nm for negative and neutral cores respectively. Furthermore, Debye-Hückel (DH) model simulations using both a fully positively charged spherical core (+62e) and with full charge on each DNA bead were also made and give results practically identical to the neutral and negative core models in a range of compaction states corresponding to $s_{20.w}$ values varying from 29S to 51S (see Fig. S11 below,). Even though the DH model is not capable of modelling effects of oligocations it reasonably well reproduces the effects of monovalent salt, and this test with variation of the central core charge, demonstrates that in the full range of nucleosome array extension from beads-on-a-string to fully folded state, the general trend of the results are not sensitive to the detailed description of the charge on the core. The inability of the DiSCO DH model (with a detailed core particle charge distribution) to capture the putative effects of interaction between the histone H4 tail and the H2A acidic patch (9), indicates that more advanced coarse graining must be developed to shed light on this issue.

In total, the 25 DNA beads carry a −236e charge, which is equal to that of the sum of the charges on 147 bp DNA (−294e) and the globular part of the histone octamer (+58e). The DNA beads are separated by 2 nm (approximately 6×0.336 nm). They wrap around the core for about 1.75 turns. This model comprises an approximate description of the shape and charge distribution of the core of the NCP. In reality, the shape of this core is more like a flat wedge-shaped cylinder. The rationale for our approach is the tremendous net negative charge of this particle, which corresponds to −236 (and with additional +88 from the tails). The electrostatic forces involved in the interaction between nucleosomes in the array are of long range. It is therefore expected that the general properties of multivalent-induced folding of the array and its dependence on the amount and charge valence of mobile counterions present, should not be highly affected by the details of the shape and charge distribution of the core particle. However, recent experimental studies have implied importance of the wedge-like NCP shape inside the so-called 30-nm chromatin fiber (10) as well as specific functions of the so-called “acidic islets” in the globular domain of the H2A histones, localized on the top and bottom of the NCP cylinder (7, 8, 11). A more refined model will be needed to describe such specific effects.

The first and the last DNA beads were placed correspondingly close to the root of H3/1 histone tail and to the root of H3/2 tail. In a local coordinate system, fixed at the NCP, the z-coordinates of the DNA beads from 1 to 9 are −1.2 nm; whereas for the DNA beads from 15 to 25, z = +1.2 nm; DNA beads 10-14 bridge two segments by being equally positioned between −1.2 nm and +1.2 nm in z-direction. The x- and y- coordinates of the DNA beads follow the circle of radius 4.45 nm with angle 26.2^o between neighboring beads. The described combination of the bead sizes and positioning closely represents the crystallographic structure of the NCP (2, 5). The integrity of the histone core and the 25 DNA beads wrapped around the central particle was maintained by assigning harmonic bonds with corresponding equilibrium distances between the DNA beads of the first and second turn and between each DNA bead and the central core particle resulting in a stable structure (Fig. S1).

The histone tails were modeled as 8 strings of linearly-connected +1e charges of effective radius 0.3 nm and bond length 0.7 nm (1, 12) (see section “Interaction potential” below for definition of effective radius). The numbers of charged particles in each tail were 9,

14, 11, and 10 for the H2A, H2B, H3 and H4 tails respectively To assign the number of charges in each of the tail, the amino acid sequences from (13) were used. Coordinates of the first (closest to the histone core) particle of each tail were chosen to match coordinates of the tail in the crystal structure of the NCP (2, 5) (Table S1).

To model the nucleosome array containing 12 nucleosomes with nucleosome repeat length 177 bp, twelve NCPs were connected by a string of five beads of 1.0 nm radius each carrying −12e charge, representing a linker DNA fragment. The distance between the beads was set to 2 nm (the same as for DNA wrapped around NCPs). The constructed nucleosome array contained 12 NCPs connected by 11×5=55 beads of linker DNA. The total charge of all DNA particles (DNA attached to the histone core plus linker DNA) was −3492e (−236e×12 + −60e×11), which combined with +1056e (+88e×12) positive charge of the histone tails gave net total charge of the whole array equal to −2436e.

TABLE S1. Coordinates (in nm) for the central particle, start/end DNA beads and the first particle at the root of each tail in the NCP model.

Particle	*x*	*y*	*z*
Core	0.0	0.0	0.0
DNA (Entry)	4.45	0	–1.20
DNA (Exit)	0	4.45	1.20
H3/1	4.80	0.0	0.0
H3/2	0.0	4.80	0.0
H2B/1	–4.00	0.0	0.0
H2B/2	0.0	–4.00	0.0
H4/1	3.10	–0.10	1.60
H4/2	–0.10	3.10	–1.60
H2A/1	–3.40	–0.10	2.10
H2A/2	–0.10	–3.40	–2.10

Interaction potential

In simulations with explicit ions, all the charged entities described above (NCP core, DNA, tails and ions) interacted by a Coulombic potential in a dielectric medium with permittivity 78. The Ewald summation method according to the P3M technique (14) was used to treat the long-range electrostatic interactions in a periodic box.

To represent steric effects, we employed a short-range variant of a Lennard-Jones potential as inter-particle potential function for every pair of particle types.

$$U_{short}(r_{ij}) = \begin{cases} \infty & r < \rho_{ij} \\ 4\varepsilon\left(\left(\frac{\sigma}{r_{ij}-\rho_{ij}}\right)^{12} - \left(\frac{\sigma}{r_{ij}-\rho_{ij}}\right)^{6} + \Delta\right) & \rho_{ij} < r < \rho_{ij} + \sqrt[6]{2}\sigma \\ 0 & r > \rho_{ij} + \sqrt[6]{2}\sigma \end{cases} \quad (1)$$

With $\varepsilon = kT = 1$; $\sigma = 0.4$ nm and shift $\Delta = 0.25\varepsilon$. In this function, the lowest point of the original Lennard-Jones curve $\left(\sqrt[6]{2}\sigma, -\varepsilon\right)$ is translated to $\left(\rho_{ij} + \sqrt[6]{2}\sigma, 0\right)$, which is also the cutoff-point for the potential energy function. This potential energy function represents a soft, purely repulsive potential, which smoothly goes down to zero at a cutoff distance $\rho_{ij} + \sqrt[6]{2}\sigma$.

The parameter ρ_{ij} for each pair of particles represents the distance of minimal approach, which is equal to the sum of "hard" radii ρ_i of each particle: $\rho_{ij}=\rho_i+\rho_j$. The typical contact distance between a pair of particles (defined by the condition that the short range potential of Eq. (1) is equal to kT) is $\rho_{ij}+\sigma$, thus the effective radius of each particle can be determined as $\rho_i + \sigma/2$. Throughout the text, "radius" of a particle means its effective radius, while the hard, or impenetrable radius of the particle is σ/2 = 0.2 nm smaller.

The particles are designated to have an effective radius according to the crystallographic structures NCP (2, 5) and DNA: histone core, 3.5 nm; DNA, 1.0 nm. The sizes of mobile ions and particles in the histone tails were set using the data of earlier Monte Carlo (15-18) simulations: tail bead, 0.3 nm; Mg^{2+}, 0.25 nm; K^+ and Cl^-, 0.2 nm; $CoHex^{3+}$, 0.35 nm.

The particles representing the amino groups of the Spd^{3+} and Spm^{4+} molecules were also attached by a harmonic bond potential ($V_{bond} = (k_{bond}/2)(r\text{-}r_0)^2$) with an equilibrium distance 4.7 Å and a force constant $k_{bond} = 10 \cdot kT$ per Å^2. A harmonic angle potential between three particles was described by an equilibrium angle of 120 degrees with a cosine potential energy of the form (k/2)(1- cos(ϕ-120^o)) with k=120·kT per rad^2. In the limit of small deviation of the angle from 120, it is equivalent to a harmonic bending potential with an angular force constant 30·kT per rad^2. The charged amino groups in Spd^{3+} and Spm^{4+} had radii 0.25 nm; the values of ρ_i are set respectively to satisfy the above effective radius. Bonds between neighboring beads of histone tails were described as in our previous work (1, 12) by a harmonic potential $(k_{bond}/2)(r\text{-}r_0)^2$ with equilibrium distance r_0 equal to 0.7 nm, and force constant $k_{bond} = 25 \cdot kT$ per Å^2.

The rigidity of DNA was described by a bending potential k/2(1 - cos ϕ), where k = 250 kT per rad^2 and ϕ is the angle between the vectors going from each "i" to "i+1", and from "i" to "i+2" beads of DNA. In the limit of small bending angle, this potential corresponds to a harmonic bending potential with angular force constant 31·kT per rad^2. Additionally, harmonic bond potentials with force constant 5·kT per Å^2 were used as flexible constraints to maintain the integrity of the NCP unit (as described in the section above). Linker DNA torsion is not included in this model, which is not addressing the issue of the details of the folded 30 nm structure.

MD simulation and trajectory analysis

Most of the MD simulation runs were carried out in a periodic cubic simulation cell with a size of 120 nm containing single "12-177" nucleosome array. The two ends of DNA going out from each NCP forms an angle 90^o, and consequently the array generated in this way adopts a "semi folded" conformation as displayed in Fig. S1. The radius of gyration for the starting structure is R_g~19 nm which is in between the extended state (R_g ~ 34 nm for the

array in K^+ salt, see Table S5-A) and fully folded state (R_g ~ 12.6 nm array in the presence of $CoHex^{3+}$, Table S5-D). For the array with monovalent (K^+) cations additional simulation runs were carried out varying the size of the simulation cell (120, 160 and 180 nm) for similar ionic strengths (see Table S5-A). It was shown that the size of the cell did not influence the behavior of the array and all calculated properties converged to similar values (see Figs. S3, S4 below). The concentration of the array in a 120 nm simulation box was 0.961 μM (about 1 μM), which corresponds to 4.024 mM in DNA phosphate groups. In most of the simulation systems, in addition to the cations neutralizing the negative charge of the array (–2436e), added salt ($M^{n+}{\cdot}nCl^-$) was present with 800 Cl^- ions corresponding to a Cl^- concentration of 0.77 mM. The influence of Mg^{2+}, $CoHex^{3+}$, Spd^{3+} and Spm^{4+} on the properties of the 12-177 nucleosome array was investigated in a number of simulations modeling substitution ("titration") of K^+ for the multivalent cations in the array solution. For pure K^+-, Mg^{2+}-, and $CoHex^{3+}$-containing systems, additional simulations were carried out with increased concentration of multivalent salt. Also, to highlight the importance of the histone tails for the chromatin folding a number of simulations runs were performed for solutions of tailless array (each NCP particle in the array was lacking the histone tails; increase of the negative charge of the array was neutralized by addition of monovalent cations in the simulation cell). The simulated systems with number of ions in the simulation cell are listed in Tables S5.

For all systems, Langevin MD simulations at 300 K were carried out using the ESPResSo package (19). In this algorithm, the total force acting on each particle, is a sum of a conservative force following from the expression for the potential energy, friction force $-\text{-}\gamma v_i$ (where γ is thermostat friction parameter and v_i is the particle velocity), and random force, the intensity of which is determined by the fluctuation-dissipation theorem (20). Masses are given in reduced units and were set to 2 for the histone tail beads, 1 for the ions, 10 for the DNA beads and to 100 for the NCP core. The ratios of the masses of the NCP core and DNA to the masses of tail beads and ions was made substantially smaller than the real ones with the purpose of providing faster sampling of the configuration space. Under assumption that the chosen reduce mass unit corresponds to 100 a.u., the time step used in simulations was equivalent 16 fs. These setting of the particle masses and thermostat parameters resulted in artificial acceleration, due to the low friction parameter (γ= 0.01) and the low mass of NCPs and may be qualitatively reconstructed by scaling the time with some factor. Since we are interested only in equilibrium configurations, we do not evaluate this factor and report only the number of MD steps made. It should be pointed out, that the configurations generated in this way are not artificial, and do represent the equilibrium ensemble for sufficient convergence of the simulation runs.

In all simulations with explicit ions, the electrostatic interactions were treated using the Ewald summation method according to the P3M technique (14). The systems were simulated for 3×10^7 – 8×10^7 MD time steps on a cluster of parallel processors at the School of Biological Sciences, Nanyang Technological University, Singapore and on the NTU High Performance Computer Centre (HPC), consisting of 2400 cores Intel Xeon 5500 series (code Nehalem) processors. Configurations for analysis were collected after each 100 steps. Average values of all parameters (sedimentation coefficient, radius of gyration, core-core contact number, various radial distribution functions) were calculated for the final 2×10^7 time steps or longer, after achieving convergence (see e.g. Fig. 2 of the Main Text and Figs. S3, S4 below).

Sedimentation coefficient was calculated in the way described in (21) using the method developed by Bloomfield et al (22) following the Kirkwood approach (23). The same approach was applied to nucleosome arrays in refs. (9) and (24). By neglecting the contribution of linker DNA, the sedimentation coefficient $S_{20,w}$ can be approximated as

$$S_{20,w} = S_1\left(1 + \frac{R_1}{N}\sum_{i>j}\frac{1}{R_{ij}}\right)$$

where summation is taken over all N=12 NCP pairs, R_{ij} is the distance between two nucleosomes, and parameters R_1 = 5.5 nm and S_1 = 11.1 Svedberg (S; 1 S = 10^{-13} sec) are adopted from previous works (9).

The radius of gyration was determined using the standard definition:

$$R_g{}^2 = \frac{1}{N}\sum_{i=1}^{N}(R_i - R_{COM})^2$$

where R_{COM} is coordinate of the center of masses of the array core particles.

Formation of histone bridges between the NCPs in the nucleosome array was characterized by the intensity of the first peak in the radial distribution functions (RDF) calculated for the central particle of each NCP in the array and particles of the external tails (external tail-core RDF). Dissociation of the tails from their own NCP was described by the intensity of the peak in the RDF calculated for the host core particle and the particles of the tails. RDF between the core particles of the NCP in the nucleosome array (core-core RDF) characterize the folding of the array. Another characteristics of the array folding, core-core contact number, is given in Tables S5. The contact number of the NCP cores is calculated from integration of the core-core RDF with $4\pi r^2$ factor over the first maximum (in the same way as coordination number is defined for simple liquids).

Fiber dimensions (diameter, length and density) were obtained by the averaged sizes of the enclosing rectangular box of the array when the array is aligned along its principal axis. The fiber axis is approximated by the principal axis of the array computed from the coordinates of NCP and linker DNA particles in the array averaged over a segment of the trajectory. The length of the fiber is taken as the height of the box, where the geometric average of the two side lengths of the box is taken as the fiber diameter.

Bulk concentration calculation

To make comparison with the experimental data one needs to estimate "bulk" concentrations of the cations which may be defined as average concentration of the ion in the region of the simulation cell with low electric field that is far away from the nucleosome array. Inside a cubic box with length 120 nm, in its extended state, the array occupies a rectangular box of 40×40×120 nm whereas it has dimensions 30×70×70 nm or less in its "semifolded" or densely compacted state. The "bulk" concentration can be measured by the density outside this "array-box". To calculate the bulk concentration, each frame of the MD trajectory was treated as follows: The array was shifted to the center of the box so that, even when the array conformation is changing from frame to frame, the "bulk" concentration is not affected. Then the density was calculated for ions in each slice 120/*n*×120×120 (n = 60 or 120, the number of slices). A bell-shape curve of cation distribution inside the simulation box with the array in the centre was usually obtained with flat lines on two sides. The average value of the ion concentration obtained from the flat curves is taken as the "bulk" ion density.

Simulations in Debye-Hückel approximation

We have also carried out a series of simulations within the Debye-Hückel approximation. In the DH simulations we use 120 nm box with periodic boundaries and minimum image convention (no Ewald summation). The array model and non-electrostatic potentials used are

the same as described above. In order to take into account the rigidity of DNA, a harmonic angle potential for each two consecutive DNA bonds $(k_{bend}/2)\cdot(\phi - \phi_0)^2$ was applied with an angular force constant $25\cdot kT$ per rad^2 and $\phi_0 = \pi$. This corresponds to the same bending rigidity of the linker DNA as used by Schlick and co-workers (21, 25-29), corresponding to a non-electrostatic persistence length, L_p, of 50 nm, based on the relation $L_p = kR_{bond}$ (R_{bond} is the bond length between DNA beads). In the DH simulations, ions were not present, and the electrostatic interactions between all charges of NCP (that is, NCP core particles, DNA and histone tail beads) were described by a screened Coulombic potential:

$$U_{DH}(r) = \frac{q_i q_j}{4\pi\varepsilon_0\varepsilon}\frac{\exp(-r/r_D)}{r}$$

With ε_0 been vacuum dielectric permittivity, ε=78 relative dielectric permittivity of water, and Debye radius r_D defined by the ion strength I:

$$r_D = \sqrt{\frac{\varepsilon_0\varepsilon kT}{2N_A e^2 I}} \quad ; \qquad I = \frac{1}{2}\sum_\alpha z_\alpha{}^2 C_\alpha$$

with z_α and C_α being the valence and concentration of α:th ion species respectively.

In simulations within the DH approximations several modifications of the above 12-177 array model were used:

1. "Neutral Core" model (the same model as used in the MD simulations with explicit ions: central core is neutral, charge of the DNA beads around the core is reduced);
2. "Positive core" model where the central particles have charge +62e (representing positive charge of the core parts of histones) while all DNA beads bear the full charge –12e;
3. "Negative Core" model where the central particle has charge –10e (the model similar to that as used in the MD simulations with explicit ions and negative charge of the central core; see above).
4. "Scaled Charge" model (all charges were scaled by factor 0.5 to illustrate the effect of charge scaling used in simulations of strongly charged polyions with a DH potential sometimes used in this approach (21, 25-29)).
5. "Tailless" model (the same tailless 12-177 nucleosome array model as used in the MD simulations with explicit ions. Tails were removed while DNA beads and core particles kept the same charges as in the NC model). The central core particle is neutral.
6. "Uncharged" model of the array: all charges on the DNA and histone tail beads were removed to simulate the array behavior in the absence of electrostatic forces.

The charge of the particles in the different models is given in Table S2 below.

The DH simulations were run for 10^7 molecular dynamics time steps of which averages were taken from the last $8\cdot10^6$ time steps.

Table S2. Charges of the particles comprising the 177-12 nucleosome array used in the MD simulations with Debye-Hückel approximation.

Particle	Full charge, neutral core	Full charge, positive core	Full charge, negative core	Scaled charge (0.5)	Tailless, neutral core
NCP core	0	+62	–10	+31	0
DNA blob attached to the core	–9.44	–12	–9.04	–6	–9.5
DNA linker blob	–12	–12	–12	–6	–12
tail monomer	+1	+1	+1	+0.5	no
Total charge of the NCP	–150	–150	–150	–75	–238

Supporting Results and Discussion

Results of sedimentation velocity studies of the 12-177-601 array in the presence of various cations

TABLE S3 Maximum concentration of cations giving reproducible sedimentation velocity curves and maximum $s_{20,w}$ values obtained in the AUC measurements.*

Added cation	Concentration, (mM)	$s_{20,w}$ (S)
Reference (TEK buffer)**	--	35.4± 0.3
K^+	100	46.9± 0.3
Na^+	100	54.5 ± 0.6
Mg^{2+}	1.0	52.5±0.7
Ca^{2+}	0.8	54.5±0.3
$Co(NH_3)_6^{3+}$	0.02	54.5±0.3
$Spermidine^{3+}$	0.06	54.8±0.5
$Spermine^{4+}$	0.002	53.25±0.5

*For all cations except TEK buffer and Mg^{2+}, the AUC experiment has been repeated twice; the data for the TEK buffer are averaging of 7 measurements; there are 5 data sets of AUC data for Mg^{2+} at 1.0 mM.

**TEK buffer: 10 mM KCl; 10 mM Tris, pH 7.6; 0.1 mM EDTA. (At pH 7.6 Tris is a mixture of protonated and basic forms with protonated form contributing 8.0 mM of the Tris cations).

Results of simulations do not depend on the size of the simulation cell.

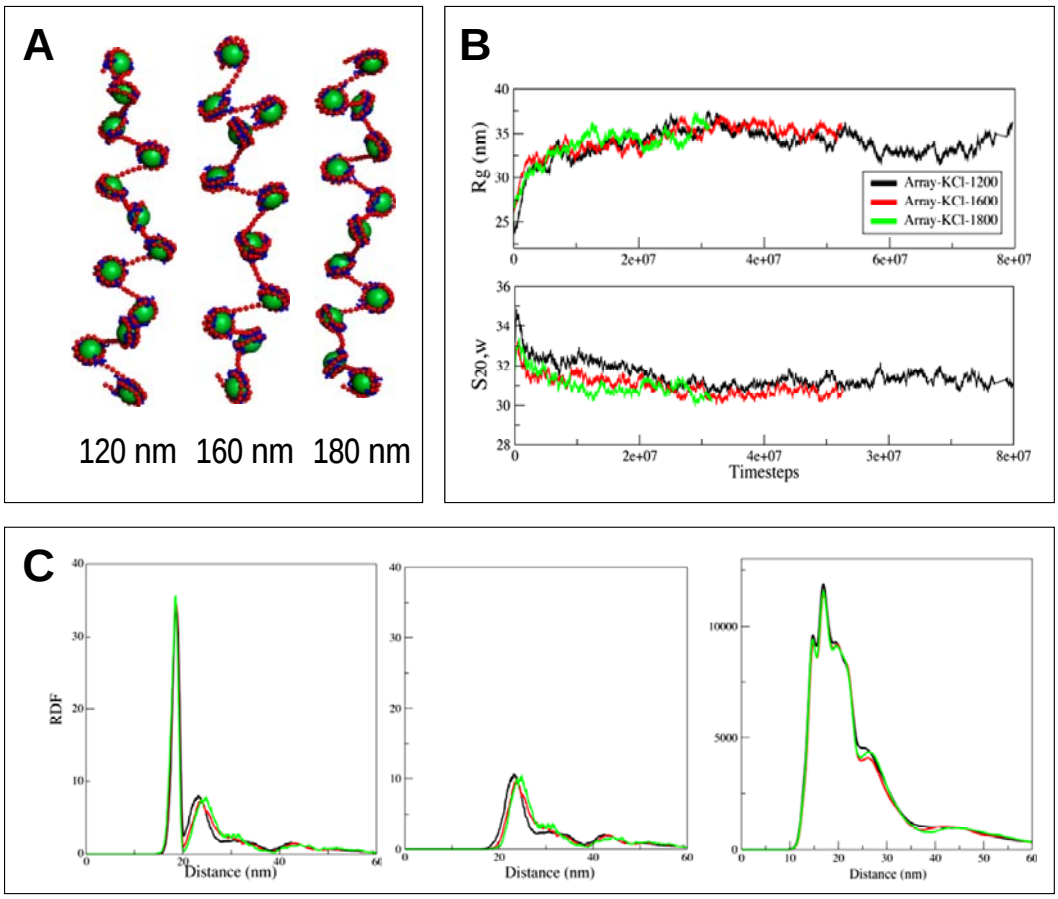

Fig. S3. Size of simulation box 120 nm is sufficient to accommodate the most extended structure of the 12-177 nucleosome array. Results of the MD simulation for the array at low concentration of KCl (0.77 mM) in the cubic simulation boxes of different size: 120, 160 and 180 nm. (**A**). Snapshots of the array at the end of the simulation run. (**B**). Variation of the radius of gyration (R_g, top graph) and sedimentation coefficient ($s_{20,w}$, bottom graph) in the course of the simulations. (**C**). RDFs calculated from the last 2×10^7 time steps of the MD simulation or longer. From left to right: core-core RDF including closest core in the array; core-core RDF excluding closest core in the array (exclusion of the closest core from the core-core distribution highlights the folding of the array); and external tails-core RDF. Number of ions and major results of the simulations are given in Table S5-A below.

Convergence of the simulations

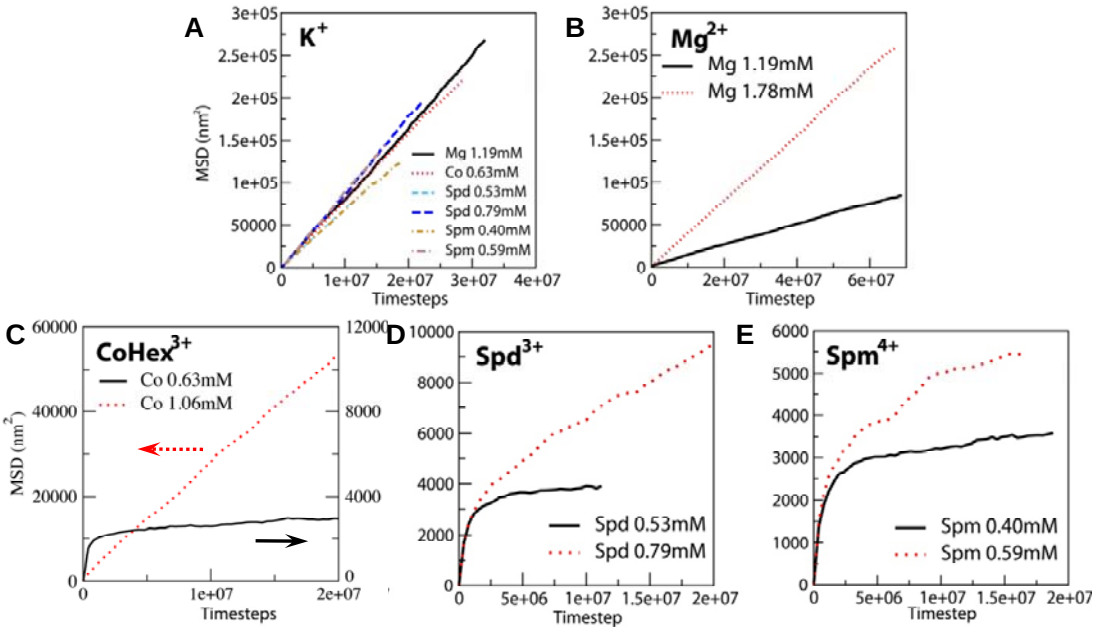

Fig. S4. Monitoring Mean Square Displacement (MSD) of the cations in the MD simulation of the 12-177 nucleosome array in the presence of various cations. (**A**) MSD of K^+ cations in titration systems containing mixture of K^+ and various concentration of Mg^{2+}, $CoHex^{3+}$, Spd^{3+} and Spm^{4+} (identity and concentration of the cations are indicated in the graph; see Tables S5 for details) (**B-E**) Variation of the MSD value in the course of the MD simulations for titration by Mg^{2+} (**B**), $CoHex^{3+}$ (**C**), Spd^{3+} (**D**), and Spm^{4+} (**E**) ions. For each cation, two curves showing MSD in the middle and in the end of the "titration" are displayed. For $CoHex^{3+}$ (**C**), scales of the y-axis are different for each $CoHex^{3+}$ concentration (indicated by arrows). Average concentration of the cation is indicated in the graphs. Note that for the highly compacted systems (end of titration) the averaged mobility of the cation is higher than that observed in the middle of titration. This reflects the fact that at the end of the "titration", where the cation concentration is relatively high, a substantial fraction of the ions are "free" and not constrained to the vicinity of the array.

The convergence of the MD simulations was checked by calculating Mean Square Displacement (MSD) of the particles as a function of the number of simulation steps. The data are summarized in Fig. S4. One can see that in all cases, including Spm^{4+}, the MSD reach a value corresponding to the square of the size of the compacted array ($50^2 = 2500$ nm^2) in less than 5×10^6 MD steps. This means that on the scale of simulations ($3\times10^7 - 8\times10^7$ MD steps) all the ions have the possibility to move along the whole array many times, which shows that sampling is adequate. In the beginning of titration at low concentration of multivalent cation, three- and higher valence ions cannot leave vicinity of the array. If the motion of ions is strictly restricted by the condition that they are always close to the array, the MSD cannot exceed the maximum distance between two distant points of the array (which is around 50-60 nm for a half-folded array). It is important that MSD reaches this distance (50^2) in a time which is short relative to the total simulation time. This means that the ions can travel many times between distant points of the array during the simulation time, providing good sampling. Mono- and divalent ions, and probably three-valent Spd^{3+}, can leave the array and go through the periodic boundaries. That is why the MSD for them is increasing with number of steps. For the mono- and divalent ions a linear regime is observed, corresponding

to the diffusion limit, the ions are not condensed on the array, they can leave it and go through periodic boundaries, which is why the MSD is proportional to time.

Results of simulations : R_g and $s_{20,w}$ trajectories, selected RDFs Mg^{2+}-titration of the 12-177 nucleosome array

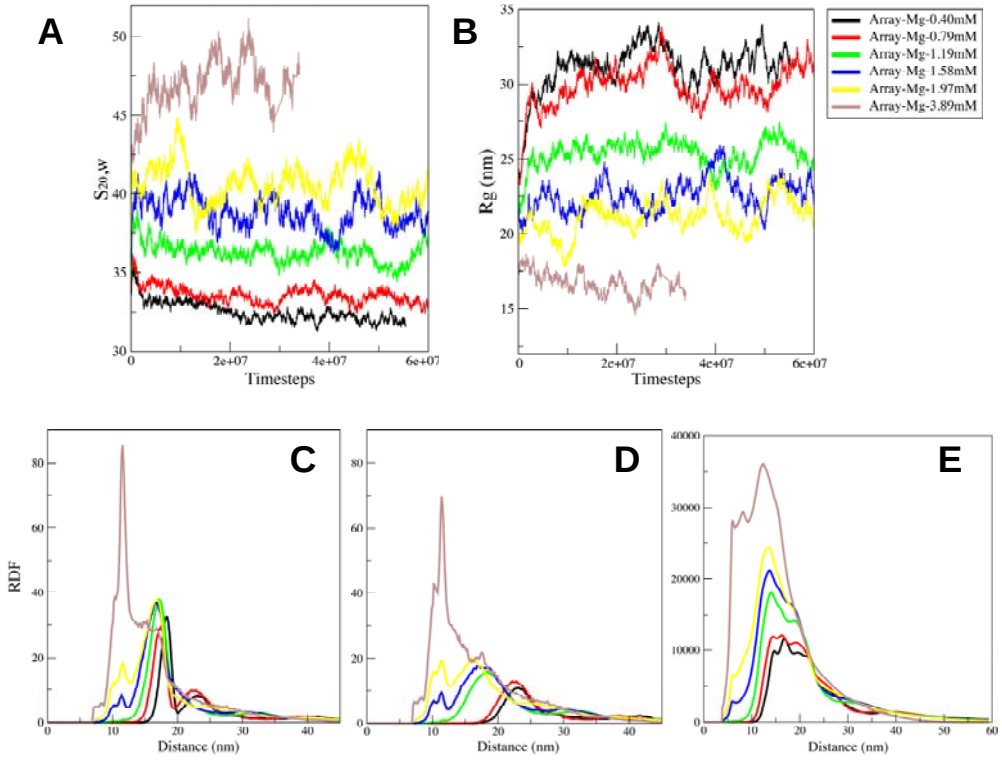

Fig. S5. Properties of the 12-177 nucleosome array in the presence of various amount of Mg^{2+}. Variation of (**A**) sedimentation coefficient, $s_{20,w}$, and (**B**) radius of gyration, R_g, in the course of the simulations (average concentration of Mg^{2+} is indicated on the right-side of the graph. (**C-E**). RDFs calculated from the last $4 \cdot 10^7$ steps of the MD simulation. From left to right: (**C**). core-core RDF including closest core in the array; (**D**). Core-core RDF excluding closest core in the array (exclusion of the closest core from the core-core distribution highlights the folding of the array); and (**E**). External tails-core RDF. Number of ions and major results of the simulations are given in Table S5-B below.

Radial distribution functions of the mobile cations

Cation-central core RDFs. In agreement with our earlier MD simulation studies of NCP-NCP interactions (1, 12) cationic species are concentrated in the vicinity of the NCP. In mixtures of mono- and multivalent cations, the cations of higher valency dominate in the vicinity of the DNA beads.

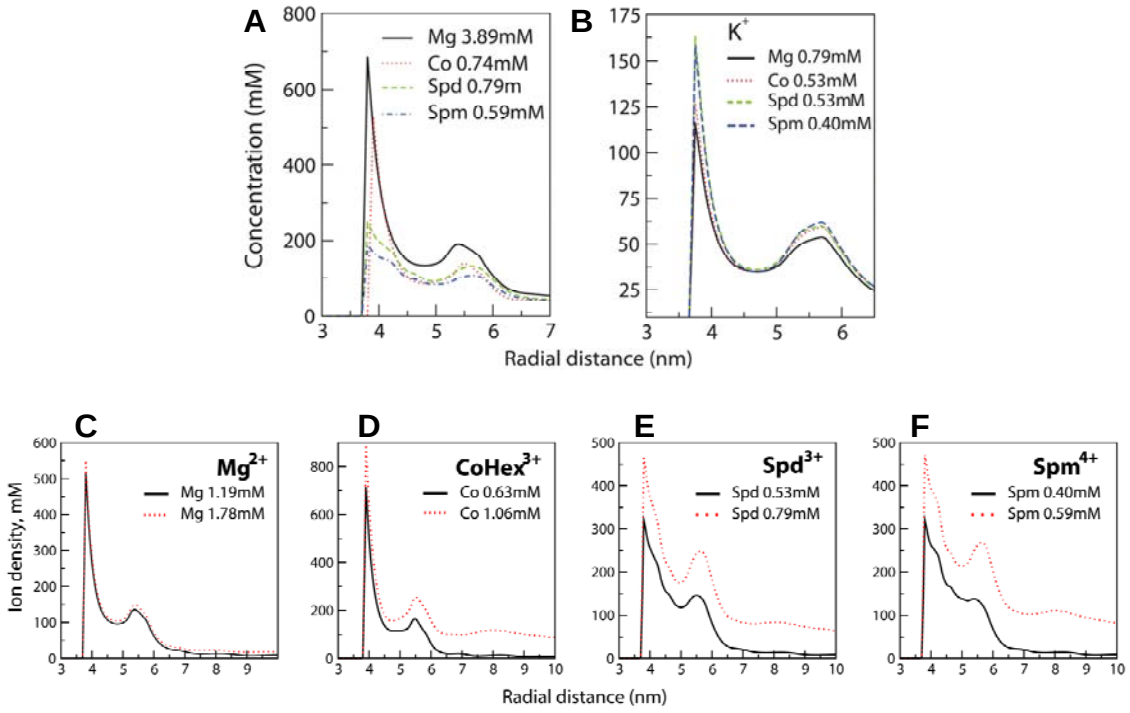

Fig. S6. Cation – central core particle radial distribution functions of multivalent cations (**A,C-F**) and K^+ (**B**) determined in the "titration" systems (multivalent cation and its average concentrations are indicated in the graph; simulated systems are specified in Tables S5 below). Graphs **C-F** show the cation-core RDFs for two mean concentrations of multivalent cation (cation identity and concentration are indicated in the graphs). RDFs were calculated from the last $4 \cdot 10^7$ steps of the MD simulation. The first maximum in the RDFs corresponds to the distance of closest ion – core particle distance; the second maximum reflects interaction of the cations with the DNA beads wrapped around the central core.

Cation-DNA RDFs.

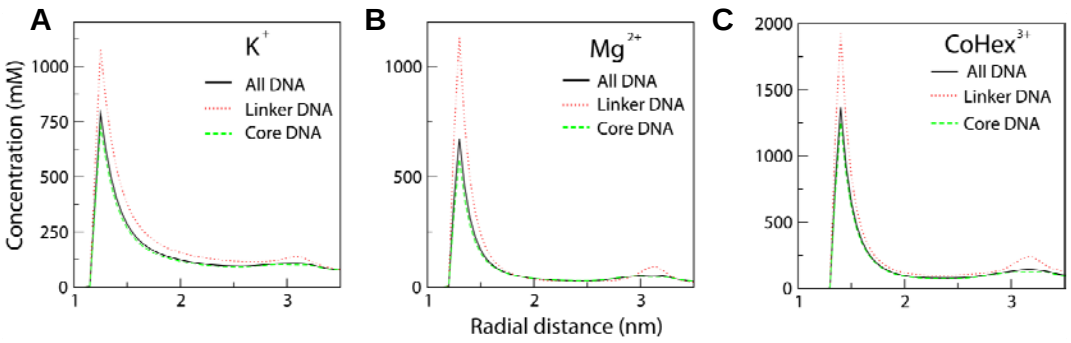

Fig. S7. Cation – DNA radial distribution functions for K^+ (**A**, C_K = 2.38 mM), Mg^{2+} (**B**, C_{Mg} = 0.40 mM) and $CoHex^{3+}$ (**C**, C_{Co} = 1.06 mM); see Tables S5 for details of the systems. The more densely charged linker DNA attracts more cations than the DNA wrapped around histone core.

Results of simulations of the Mg^{2+}-, $CoHex^{3+}$-, Spd^{3+}- and Spm^{4+}-titration of the 12-177 nucleosome array

Mg^{2+}- and $CoHex^{3+}$-titrations: Dependencies of $s_{20,w}$, R_g, and intensity of the external tail – core RDF maximum on average concentration of the oligocation.

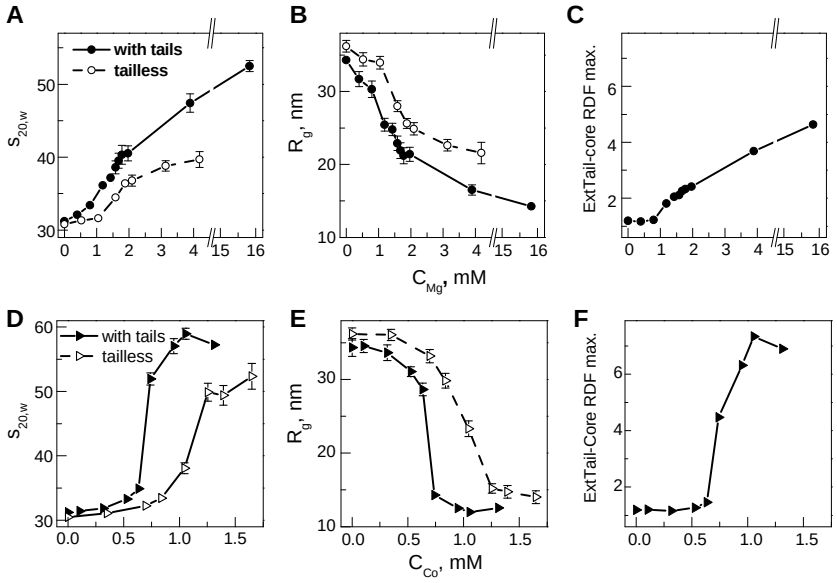

Fig. S8. Properties of the 12-177 nucleosome array in the presence of Mg^{2+} (**A-C**) and $CoHex^{3+}$ (**D-F**) as a function of averaged concentration of the oligocation. Variation of (**A,D**) sedimentation coefficient, $s_{20,w}$; (**B,E**) radius of gyration, R_g,; and (**C,F**) intensity of the maximum in the external tail-core RDF. Dependencies of the same parameters on "bulk" concentration of the oligocation are given in Fig. 3 of the Main Text (for Mg^{2+}- and $CoHex^{3+}$-titrations).

Spd^{3+}- and Spm^{4+}-titration: Dependencies of $s_{20,w}$, R_g, and intensity of the external tail-core RDF maximum on average concentration of the oligocation.

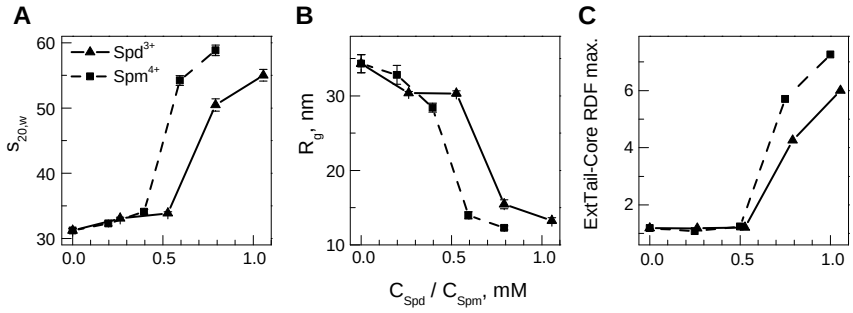

Fig. S9. Properties of the 12-177 nucleosome array in the presence of Spd^{3+} and Spm^{4+} as a function of average concentration of the oligocation. Variation of (**A**) sedimentation coefficient, $s_{20,w}$; (**B**) radius of gyration, R_g,; and (**C**) intensity of the maximum in the external tail-core RDF. Dependencies of the same parameters on bulk concentration of the oligocations are given in Fig. 3 of the Main Text. (for Spd^{3+}- and Spm^{4+}-titrations).

Analysis of internal structures of the 12-177 nucleosome array obtained in the simulations

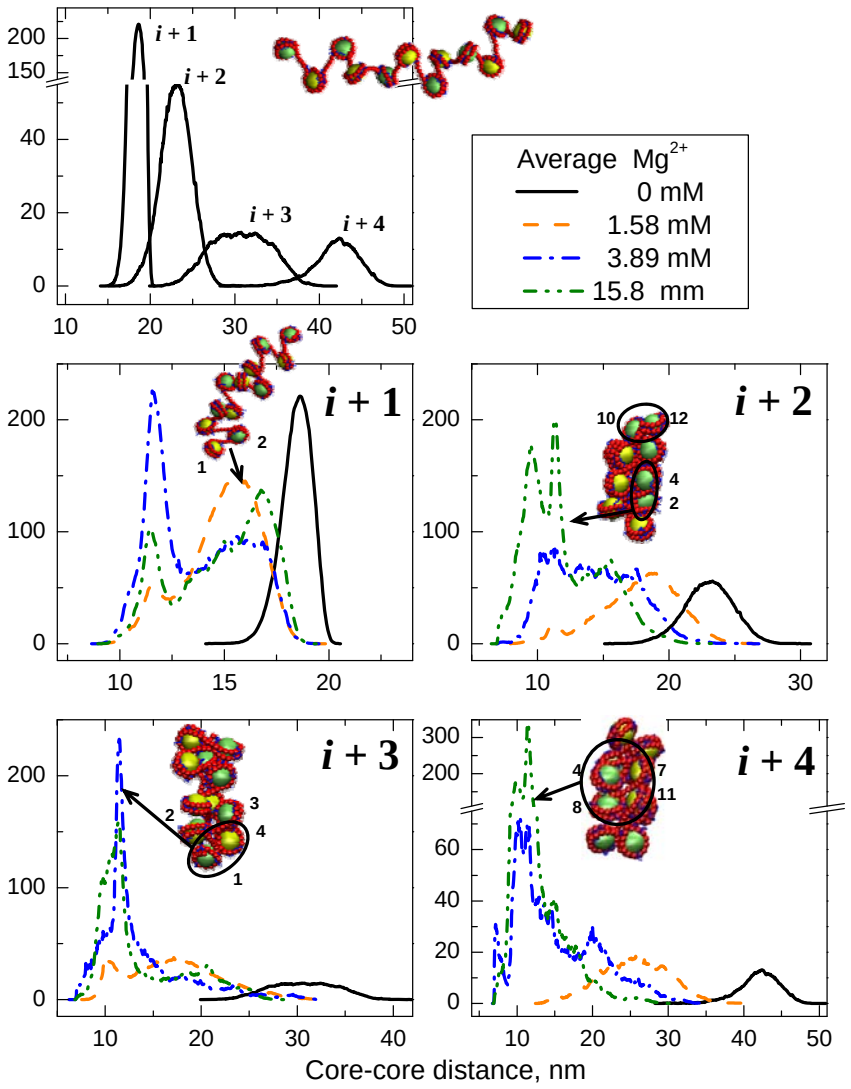

Fig. S10. Analysis of internal structure of the 12-177 nucleosome array in the presence of various concentration of Mg^{2+}. The top graph illustrate core-core distance distribution calculated for differently separated core particles in the extended array (C_{Mg} = 0, Table S5-B, 1st line); the four panels below compare core-core distance distributions obtained with different concentration of Mg^{2+} (indicated in the graph) for similar pairs of core particles; neighboring (i+1); separated by one (i+2); two (i+3) and three (i+4) particles. Snapshots illustrate typical cases of core-core positioning in the array.

In the presence of low concentration of monovalent salt, the array adopts an extended conformation with core-core distribution showing increased distance with increase of the separation between the cores (Fig. S10, top graph). Upon addition of Mg^{2+}, the array experiences folding which results in a decrease of the distance between the neighboring particles due to increase of flexibility of the linker DNA (top-left graph, orange dashed curve and snapshot). Clearly, the other core-core distances are also decreasing due to the fiber folding (orange dashed curves in the graphs). Detailed inspection of many snapshots reveals that the array folds in a zigzag like manner. At high concentration of Mg^{2+} (C_{Mg} = 3.89 and

15.83 mM) the arrays adopt folded conformations with multiple close core-core contacts showing features characteristic of the two-start zigzag model. This model expects close contacts for *i*+2 distribution as illustrated in the corresponding graph and snapshot (core particles with even and odd number are colored differently). At the same time, irregular contacts like *i*+3 are also frequent as illustrated in the bottom-left graph for the case C_{Mg} = 3.89 mM when the fiber is not yet fully compact. In agreement with the results of chromatin fiber modeling by Schlick and co-authors (28), we also observed high frequency of *i*+4 contacts which was explained by the intrinsic geometry of the array with entry-exit 90^o angle between linker DNAs.

In general the fiber appearance bears some similarity with electron microscopy images reported in literature (e.g. (30) where longer (80 NCPs) arrays with 167bp NRL were visualized in the absence and in the presence of linker histone with fiber diameter in the range 18-25 nm and array linear density 5-7 NCP/11 nm). We made a statistical analysis of the fiber parameters for concentrations corresponding to compact arrays in the systems of all four cations (see Table S7 below). For Mg^{2+} in the most compact state, the fiber diameter is about 24 nm and the nucleosome density is about 4.1 (per 11 nm) (Table S7) for analysis excluding the first and last three nucleosomes. Including the ends significantly decrease the density, see Table S7, demonstrating the end effects. This fiber width is close to the 25 nm expected for an idealized two-start model, while the density predicted from the tetranucleosome structure is about 5.8 nucleosome/(11 nm) (31). The discrepancy in density is likely due to end effects for the present short array and is also strongly influenced by the lack of close stacking imposed by our spherical core model. In the presence of the cations of higher valence, more compact globular states are formed (Table S7 below; see also Fig. 3 of the Main Text). Little is known about chromatin structure in the presence of multivalent ions, but due to strong binding, more compact fibers would be expected.

Results of MD simulations in Debye-Hückel approximation

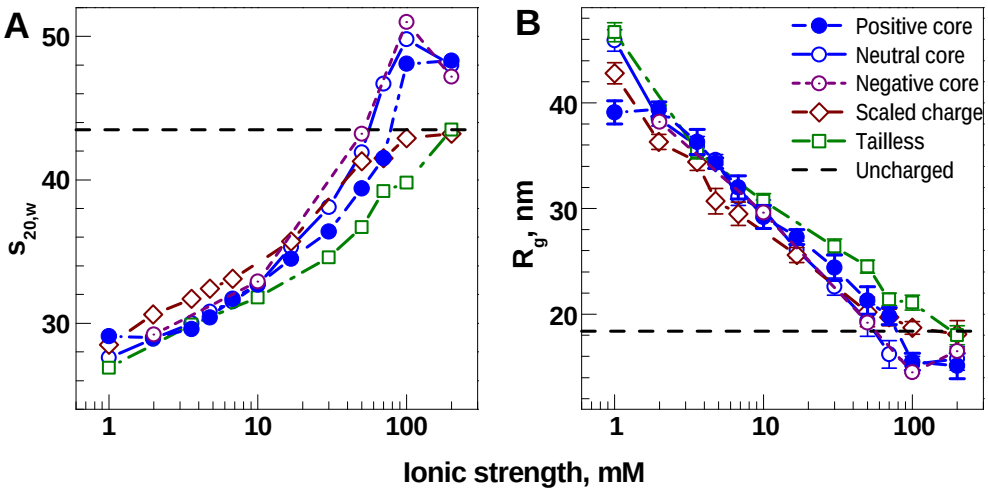

Fig. S11. Results of the MD simulations within Debye-Hückel approximation as a function of ionic strength for different models of the array. (**A**) Sedimentation coefficient, $s_{20,w}$; (**B**) radius of gyration, R_g. Horizontal dashed lines indicate the values of $s_{20,w}$ and R_g calculated for the array model with uncharged particles. Description of the array models is given in Supporting Computational Methods section above (Table S2). In the range of ionic strength from 1 to 200 mM, array models using positive, neutral or negative charge of the central particle give similar values of sedimentation coefficient and radius of gyration. At high ionic strength, the model with all charges of the particles reduced to 50% and the tailless array model show folding equal or below to that calculated for the uncharged array. See Fig. 4 of the Main Text for comparison with experimental data and with the results of the MD simulations with explicit ions

The Debye-Hückel approximation cannot take into account most of electrostatic contributions to chromatin folding

As specified in Table S4 below, different contributions of electrostatic origin to chromatin statics and dynamics may be divided on: cation-anion Coulombic interactions, screening and DNA charge neutralization, cation multi-valency and structure, mobile ion correlations, tail-tail correlations and tail bridging effects.

TABLE S4 Modeling of electrostatic contributions to chromatin folding

Model	Electrostatic contribution					
	Cation-anion interactions	Screening /charge neutra-lization	Cation multi-valency/ structure	Mobile ion correlations	Tail-tail corrélations	Tail bridging
	1	**2**	**3**	**4**	**5**	**6**
Array with charged tails; explicit ions	+	+	+	+	+	+
Tailless array; explicit ions	+	+	+	+	–	–
Array with charged tails; Debye-Hückel approximation	+/–*	+/–*	–	–	+/–*	+/–*
Tailless array; Debye-Hückel approximation	–	+/–*	–	–	–	–
Array without charges	–	–	–	–	–	–

***** **+/–** means this type of interaction is included, but incompletely.

1 Cation-anion attraction: Attractive potential arising from the cation-anion Coulombic interaction.

2 Screening/charge neutralization: Decrease of the repulsion between similarly charged particles originated from delocalized presence of the counterions (screening) and direct binding of the oppositely charged ligand (charge neutralization).

3 Cation multivalency/structure: Ability of the model to explicitly take into account multivalency and chemical structure of the cation species.

4 Mobile ion correlations: Dynamic correlation of the fluctuated delocalized binding of the mobile counterions to the neighboring polyions (like NCP or linker DNA).

5 Tail-tail correlations: The same as mobile ion correlations but applied to the histone tails of the neighboring NCPs.

6 Tail bridging: Binding of the histone tails to the neighboring NCP and to the linker DNA.

All the above listed contribution are either absent or lack adequate representation within chromatin models based on Debye-Hückel approximation. Referring to Table S4, we may compare these contributions to the electrostatic mechanism of chromatin folding as it emerges from the presentation of the combined results from our experiments and the theoretical modeling. The first mechanism, cation-anion interactions may be considered as the static Coulombic interaction between positively (histone tails and mobile cations) and negatively (mainly DNA) charged units in a given configuration. It is partly described in DH models since there are no explicit mobile cations in this treatment. The DH treatment with charged histone tails includes tail-DNA interactions. Screening/charge neutralization refers to the reduction in electrostatic interactions due to the ion atmosphere and counterion condensation and binding on the DNA polyelectrolyte, leading to an effective neutralization

of its negative charge. This is present in the full explicit ion as well as partly in the DH models. The importance of counterion release, which is absent in the DH descriptions, is mostly ignored in the context of chromatin, but is a well-known entropy effect for DNA condensation (32, 33). It is the entropy gain due to the monovalent ion release caused by an increased oligocation association to DNA in the collapsed state (as compared to the random coil). The cation multivalency/structure refers to effect of the chain-like structure of the polyamine oligocations and accounts for differences between oligocations of the same charge, but of different nature (e.g. $CoHex^{3+}$ and Spd^{3+}). The mobile ion correlations is probably the most important contribution to attraction between nucleosomes neglected in the DH/PB models. The tail-tail correlations refers to the contribution caused by attractions induced by the correlated fluctuations in the positions of tails belonging to different nucleosomes and is included in both treatments if a charged flexible tail model is used. However, a DH treatment is approximate in this respect since this correlation is coupled to correlations with small mobile ions, while in the DH treatment it always occur on the background of a screened interaction. Tail bridging, which is not clearly distinguished from the tail-tail correlation, refers to the entropy gain upon tail binding to negatively sites on adjacent nucleosomes rather than its own core. This mechanism is clearly observed by the increase in the intensity of the external tail-core RDFs upon folding (Fig 3 of the Main Text). This interaction is also incompletely described in a DH model for the same reasons as just mentioned in the case of tail-tail correlations.

Table S5. Summary of simulations for the 12-177 nucleosome array.

(* see more explanation at the bottom of Table S5-A)

Table S5-A. Monovalent (K^+) cations

Cell size, nm	Number of ions		Average K^+, mM	Bulk K^+, mM	Ionic strength, mM	Sedimentation coefficient, S	Radius of gyration, nm	Core-core contact number	RDF maximum, rel. units	
	K^+	Cl^-							ExtTail-core	IntTail-core
180	5196	2700	1.48	0.804	1.12	30.8±0.3	34.6±1.1	3.07	1.15	74.0
160	4392	1896	1.78	0.812	1.27	30.7±0.3	35.6±0.8	2.92	1.15	74.1
120	3296**	800	3.17	0.874	1.97	31.2±0.3	34.3±1.2	2.88	1.19	74.0
120	7496	5000	7.20	4.879	6.00	34.1±0.4	28.9±0.9	3.91	1.53	73.0

** Concentration of 2496 K^+ ions neutralizing negative charge of the array is 2.34 mM

* "Bulk" concentration of the given cation was determined as described in the Computational Method section above. Total charge of the DNA (number of the phosphate groups) in the 12-177 array is 12x294 + 11x60 = 4158. For the box 120 nm used in the most of the simulations (volume 1.728×10^{-18} liter) concentration of the array is 0.96096 μM (one particle per cell), C_P = 4.024 mM. The histones neutralize charge of the DNA wrapped in the NCP from –294 to –236 (–294 + 58) and this neutralization is accounted by assigning charge –9.44 to each of the 25 DNA beads ; additionally NCP carries the tails of positive charge +88. As a result net charge of the array is –236x12 + –60x11 + 88x11 = –3492 + 1056 = –2436; that gives concentration of the negative charge in the 120 nm box 2.34 mM and degree of neutralization of the DNA charge (combined neutralization from the globular histones and the histone tails) 0.4141 so 58.59% of the DNA charge remains un-neutralized by the histones. For the tailless array in the 120 nm cell, C_P remains the same C_P = 4.024 mM but DNA is neutralized only by the globular histones so 12-177 array carries the charge –3492 (concentration of the negative charge 3.356 mM; neutralization of the DNA charge is equal to 0.1602, so 83.98% of the DNA charge remains un-neutralized by the histones.

Table S5-B. Array with histone tails; Mg^{2+} titration

Number of ions		Average	Bulk Mg^{2+},	Ionic	Sedimentation	Radius of	Core-core contact	RDF maximum, rel. units	
K^+	Mg^{2+}	Mg^{2+}, mM	mM	strength, mM	coefficient, S	gyration, nm	number	ExtTail-core	IntTail-core
3296*	0	0.0	0.0	1.97	31.2±0.3	34.3±1.2	2.88	1.19	74.0
2472	412	0.40	0.0001	2.36	32.1±0.3	31.7 ± 1.05	3.21	1.17	64.4
1648	824	0.79	0.0066	2.76	33.4±0.4	30.3 ± 1.1	3.92	1.22	57.0
824	1236	1.19	0.113	3.16	36.1±0.6	25.45 ± 0.9	4.61	1.81	52.5
330	1483	1.43	0.280	3.39	37.2±0.7	24.8 ± 0.85	5.09	2.05	51.6
0	1648	1.58	0.426	3.55	38.6±0.9	22.9 ± 1.0	5.71	2.11	51.3
0	1748	1.68	0.514	3.84	39.5±1.0	21.9 ± 1.1	6.12	2.26	51.1
0	1848	1.78	0.595	4.13	40.3±1.3	21.2 ± 1.1	6.56	2.33	50.9
0	2048	1.97	0.809	4.70	40.5±1.0	21.4 ± 1.0	6.62	2.41	50.6
0	4048	3.89	2.696	10.47	47.4±1.3	16.5±0.7	8.25	3.68	48.0
0	16474	15.83	14.75	46.29	52.5±0.8	14.3±0.4	8.13	4.63	45.1

Table S5-C. Tailless array; Mg^{2+} titration*

Number of ions		Average	Bulk Mg^{2+},	Ionic strength,	Sedimentation	Radius of	Core-core contact
K^+	Mg^{2+}	Mg^{2+}, mM	mM	mM	coefficient, S	gyration, nm	number
4352	0	0.00	0.0	2.48	30.7 ±0.3	36.2 ± 0.8	2.15
3264	544	0.52	0.000054	3.00	31.3± 0.2	34.4 ± 0.9	2.29
2176	1088	1.05	0.00244	3.52	31.6 ±0.3	34.0 ± 0.9	2.53
1088	1632	1.57	0.058	4.04	34.5± 0.4	28.0 ± 0.7	3.26
436	1958	1.88	0.220	4.36	36.4 ±0.5	25.6 ± 0.7	3.79
0	2176	2.09	0.432	4.57	36.8± 0.7	24.9± 0.9	3.93
0	3264	3.14	1.440	7.70	38.8± 0.7	22.6± 0.8	4.50
0	4352	4.18	2.500	10.84	39.7± 1.1	21.6± 1.5	4.94

*Concentration negative charge of the tailless array is 3.356 mM (in charge units)

Table S5-D. Array with histone tails; $CoHex^{3+}$ titration

Number of ions		Average $CoHex^{3+}$, mM	Bulk $CoHex^{3+}$, μM	Ionic strength, mM	Sedimentation coefficient, S	Radius of gyration, nm	Core-core contact number	RDF maximum, rel. units	
K^+	$CoHex^{3+}$							ExtTail-core	IntTail-core
3296*	0	0.0	0.0	1.97	31.2±0.3	34.3±1.2	2.88	1.19	74.0
2966	110	0.11	0.28	2.29	31.4±0.3	34.5 ± 0.9	2.68	1.20	68.9
2309	329	0.32	0.53	2.92	31.8±0.4	33.6 ± 1.1	3.12	1.16	61.8
1649	549	0.53	1.105	3.55	33.3±0.4	31.1 ± 0.7	3.68	1.27	55.3
1319	659	0.63	1.27	3.87	34.9±0.4	28.7 ± 0.9	4.11	1.46	52.0
989	769	0.74	2.35	4.18	51.9±0.9	14.3 ± 0.5	10.73	4.47	45.8
329	989	0.95	154.2	4.82	57.0±1.2	12.5 ± 0.5	11.63	6.31	43.4
2	1098	1.06	284.0	5.13	58.95±0.9	12.0 ± 0.3	11.95	7.33	42.8
0	1365	1.31	500.0	6.67	57.2±0.6	12.6 ± 0.2	11.70	6.90	43.0

Table S5-E. Tailless array; $CoHex^{3+}$ titration

Number of ions		Average $CoHex^{3+}$, mM	Bulk $CoHex^{3+}$, μM	Ionic strength, mM	Sedimentation coefficient, S	Radius of gyration, nm	Core-core contact number
K^+	$CoHex^{3+}$						
4352	0	0.00	0.0	2.48	30.7 ±0.3	36.2 ± 0.8	2.15
3264	363	0.35	0.202	3.52	31.1±0.3	36.1 ± 0.75	2.80
2177	725	0.70	0.576	4.57	32.2±0.4	33.2 ± 0.9	2.80
1740	871	0.84	0.721	4.99	33.4±0.3	29.8 ± 1.0	3.94
1088	1088	1.05	1.153	5.61	38.1±0.9	23.3 ± 1.1	5.61
435	1306	1.26	126.3	6.24	49.9±1.4	15.2 ± 0.6	10.36
0	1451	1.39	275.5	6.66	49.4±1.5	14.7 ± 0.9	10.56
0	1717	1.65	524.1	8.19	52.4±2.0	14.0 ± 0.9	11.12

Table S5-F. Array with histone tails; Spermidine^{3+} titration

Number of cations		Average Spd^{3+}, mM	Bulk Spd^{3+}, μM	Ionic strength, mM	Sedimentation coefficient, S	Radius of gyration, nm	Core-core contact number	RDF maximum, rel. units	
K^+	Spd^{3+}							ExtTail-core	IntTail-core
3296*	0	0.0	0.0	1.97	31.2±0.3	34.3±1.2	2.88	1.19	74.0
2474	274	0.26	0.0769	2.76	33.1±0.2	30.4 ± 0.2	3.91	1.18	68.2
1649	549	0.53	0.2857	3.55	33.9±0.2	30.3± 0.4	4.03	1.21	64.0
824	824	0.79	30.83	4.34	50.5±1.0	15.5± 0.6	9.89	4.26	55.3
0	1099	1.06	256.8	5.14	55.0±0.9	13.3± 0.4	11.54	6.00	54.1
No tails, 0	1451	1.39	261.1	6.66	45.7±1.4	18.2± 0.9	8.39	---	---

Table S5-G. Array with histone tails; Spermine^{4+} titration

Number of cations		Average Spm^{4+}, mM	Bulk Spm^{4+}, μM	Ionic strength, mM	Sedimentation coefficient, S	Radius of gyration, nm	Core-core contact number	RDF maximum, rel. units	
K^+	Spm^{4+}							ExtTail-core	IntTail-core
3296*	0	0.0	0.0	1.97	31.2±0.3	34.3±1.2	2.88	1.19	74.0
2472	206	0.20	0.0505	3.16	32.3±0.4	32.8 ± 1.3	3.44	1.08	66.7
1648	412	0.40	0.1441	4.34	34.1±0.4	28.4 ± 0.6	4.33	1.24	61.1
824	618	0.59	3.114	5.53	54.2±0.8	14.0 ± 0.5	10.75	5.70	51.6
0	824	0.79	209.3	6.72	58.8±0.8	12.3 ± 0.3	11.74	7.26	51.5
No tails, 0	1088	1.05	198.9	8.75	54.3±1.3	13.6 ± 0.6	11.11	---	---

Table S6. Selected results from MD simulations of arrays using Debye-Hückel approximation. MD simulations of the uncharged model of the 12-177 array give R_g = 18.4 ± 1.0 nm and $s_{20,w}$ = 43.5; results obtained for the array models with negative and positive charge of the central particle are shown in Fig. S10 above.

Ionic strength, mM	Full charge, neutral core		Scaled charge (0.5)		Tailless, neutral core	
	R_g, nm	$s_{20,w}$	R_g, nm	$s_{20,w}$	R_g, nm	$s_{20,w}$
1.0	45.9 ± 1.0	27.6	42.8 ± 1.0	28.5	46.7 ± 0.9	26.9
1.98	38.5 ± 0.7	28.9	36.3 ± 0.7	30.6	--	--
3.59	35.9 ± 0.9	30.	34.4 ± 0.8	31.7	35.4 ± 0.7	29.9
4.75	34.6 ± 0.5	30.8	30.7 ± 1.2	32.4	--	--
6.79	31.1 ± 0.8	31.5	29.5 ± 1.1	33.1	--	--
10.0	29.9 ± 0.9	32.7	--	--	30.7 ± 0.7	31.8
16.7	26.1 ± 0.8	35.3	25.6 ± 0.7	35.7	--	--
30	22.6 ± 0.8	38.1	--	--	26.4 ± 0.7	34.6
50	19.4 ± 1.5	41.9	20.2 ± 1.4	41.3	24.5 ± 0.6	36.7
70	16.2 ± 1.3	46.7	19.7 ± 0.8	41.5	21.4 ± 0.6	39.2
100	15.2 ± 0.8	49.8	18.7 ± 0.6	42.9	21.1 ± 0.7	39.8
200	15.8 ± 1.1	48.0	18.1 ± 1.3	43.2	18.0 ± 0.9	43.5

Table S7. Fiber dimensions for compact 12-177 arrays calculated from the analysis of the MD simulations
Analysis excluding the ends (first and last three nucleosomes):

Cation	Concentration. (mM)	Fiber length (nm)	Fiber width (nm)	Density (Nucleosome/11 nm)
Mg^{2+}	3.89	48.6	25.02	4.14
	15.84	47.1	24.04	4.07
$CoHex^{3+}$	0.74	53.7	26.42	2.78
	0.95	33.4	21.90	4.23
	1.06	39.6	22.09	4.76
	1.31	42.8	23.20	4.72
Spd^{3+}	0.79	48.1	22.56	4.30
	1.06	37.5	24.24	4.67
Spm^{4+}	0.59	39.5	22.69	4.07
	0.79	36.1	22.30	4.58

Analysis based on all 12 nucleosomes:

Cation	Concentration (mM)	Fiber length (nm)	Fiber width (nm)	Density (Nucleosome/11 nm)
Mg^{2+}	3.89	48.6	29.2	2.7
	15.84	47.1	26.5	2.8
$CoHex^{3+}$	0.74	53.7	28.4	2.5
	0.95	33.4	27.0	4.0
	1.06	39.6	24.2	3.3
	1.31	42.8	25.9	3.1
Spd^{3+}	0.79	48.1	26.7	2.7
	1.06	37.5	25.5	3.5
Spm^{4+}	0.59	39.5	27.8	3.3
	0.79	36.1	25.5	3.7

References

1. Yang, Y., A. P. Lyubartsev, N. Korolev, and L. Nordenskiöld. 2009. Computer modeling reveals that modifications of the histone tail charges define salt-dependent interaction of the nucleosome core particles. *Biophys.J.* 96:2082-2094.
2. Davey, C. A., D. F. Sargent, K. Luger, A. W. Maeder, and T. J. Richmond. 2002. Solvent mediated interactions in the structure of nucleosome core particle at 1.9 Å resolution. *J.Mol.Biol.* 319:1097-1113.
3. Arents, G., and E. N. Moudrianakis. 1993. Topography of the histone octamer surface: repeating structural motifs utilized in the docking of nucleosomal DNA. *Proc.Natl.Acad.Sci.U.S.A.* 90:10489-10493.
4. Cherstvy, A. G. 2009. Positively charged residues in DNA-binding domains of structural proteins follow sequence-specific positions of DNA phosphate groups. *J.Phys.Chem.B* 113:4242-4247.
5. Luger, K., A. W. Mader, R. K. Richmond, D. F. Sargent, and T. J. Richmond. 1997. Crystal structure of the nucleosome core particle at 2.8 Å resolution. *Nature* 389:251-260.
6. Luger, K., and T. J. Richmond. 1998. The histone tails of the nucleosome. *Curr.Opin.Genet.Dev.* 8:140-146.
7. Chodaparambil, J. V., A. J. Barbera, X. Lu, K. M. Kaye, J. C. Hansen, and K. Luger. 2007. A charged and contoured surface on the nucleosome regulates chromatin compaction. *Nat. Struct. Mol. Biol.* 14:1105-1107.
8. Zhou, J., J. Y. Fan, D. Rangasamy, and D. J. Tremethick. 2007. The nucleosome surface regulates chromatin compaction and couples it with transcriptional repression. *Nat. Struct. Mol. Biol.* 14:1070-1076.
9. Garcia-Ramirez, M., F. Dong, and J. Ausio. 1992. Role of the histone "tails" in the folding of oligonucleosomes depleted of histone H1. *J.Biol.Chem.* 267:19587-19595.
10. Robinson, P. J. J., L. Fairall, V. A. T. Huynh, and D. Rhodes. 2006. EM measurements define the dimensions of the "30-nm" chromatin fiber: Evidence for a compact, interdigitated structure. *Proc.Natl.Acad.Sci.U.S.A.* 103:6506-6511.
11. Barbera, A. J., J. V. Chodaparambil, B. Kelley-Clarke, V. Joukov, J. C. Walter, K. Luger, and K. M. Kaye. 2006. The nucleosomal surface as a docking station for Kaposi's sarcoma herpesvirus LANA. *Science* 311:856-861.
12. Korolev, N., A. P. Lyubartsev, and L. Nordenskiöld. 2006. Computer modeling demonstrates that electrostatic attraction of nucleosomal DNA is mediated by histone tails. *Biophys.J.* 90:4305-4316.
13. Cheung, P., C. D. Allis, and P. Sassone-Corsi. 2000. Signaling to chromatin through histone modification. *Cell* 103:263-271.
14. Deserno, M., and C. Holm. 1998. How to mesh up Ewald sums. I. A theoretical and numerical comparison of various particle mesh routines. *J.Chem.Phys.* 109:7678-7693.
15. Lyubartsev, A. P., and L. Nordenskiöld. 1997. Monte Carlo simulation study of DNA polyelectrolyte properties in the presence of multivalent polyamine ions. *J.Phys.Chem.B* 101:4335-4342.
16. Korolev, N., A. P. Lyubartsev, L. Nordenskiöld, and A. Laaksonen. 2001. Spermine: an "invisible" component in the crystals of *B*-DNA. A grand canonical Monte Carlo and molecular dynamics simulation study. *J.Mol.Biol.* 308:907-917.

17. Korolev, N., A. P. Lyubartsev, A. Rupprecht, and L. Nordenskiöld. 1999. Competitive binding of Mg^{2+}, Ca^{2+}, Na^{+}, and K^{+} to DNA in oriented DNA fibers: experimental and Monte Carlo simulation results. *Biophys.J.* 77:2736-2749.
18. Korolev, N., A. P. Lyubartsev, A. Rupprecht, and L. Nordenskiöld. 2001. Competitive substitution of hexammine cobalt(III) for Na^{+} and K^{+} ions in oriented DNA fibers. *Biopolymers* 58:268-278.
19. Limbach, H. J., A. Arnold, B. A. Mann, and C. Holm. 2006. ESPResSo - an extensible simulation package for research on soft matter systems. *Comp.Phys.Comm.* 174:704-727.
20. Grest, G. S., and K. Kremer. 1986. Molecular dynamics simulation for polymers in the presence of a heat bath. *Phys.Rev. A* 33:3628-3631.
21. Sun, J., Q. Zhang, and T. Schlick. 2005. Electrostatic mechanism of nucleosomal array folding revealed by computer simulation. *Proc.Natl.Acad.Sci.U.S.A.* 102:8180-8185.
22. Bloomfield, V., W. O. Dalton, and K. E. Van Holde. 1967. Frictional coefficients of multisubunit structures. I. Theory. *Biopolymers* 5:135-148.
23. Kirkwood, J. G. 1954. The general theory of irreversible processes in solutions of macromolecules. *J.Polym.Sci.* 6:1-14.
24. Hansen, J. C., J. Ausio, V. H. Stanik, and K. E. van Holde. 1989. Homogeneous reconstituted oligonucleosomes, evidence for salt-dependent folding in the absence of histone H1. *Biochemistry* 28:9129 - 9136.
25. Zhang, Q., D. A. Beard, and T. Schlick. 2003. Constructing irregular surfaces to enclose macromolecular complexes for mesoscale modeling using the discrete surface charge optimization (DiSCO) algorithm. *J.Comp.Chem.* 24:2063-2074.
26. Arya, G., Q. Zhang, and T. Schlick. 2006. Flexible histone tails in a new mesoscopic oligonucleosome model. *Biophys.J.* 91:133-150.
27. Arya, G., and T. Schlick. 2006. Role of histone tails in chromatin folding revealed by a mesoscopic oligonucleosome model. *Proc.Natl.Acad.Sci.U.S.A.* 103:16236-16241.
28. Grigoryev, S. A., G. Arya, S. Correll, C. L. Woodcock, and T. Schlick. 2009. Evidence for heteromorphic chromatin fibers from analysis of nucleosome interactions. *Proc.Natl.Acad.Sci.U.S.A.* 106:13317–13322.
29. Arya, G., and T. Schlick. 2009. A tale of tails: How histone tails mediate chromatin compaction in different salt and linker histone environments. *J.Phys.Chem.A* 113:4045-4059.
30. Routh, A., S. Sandin, and D. Rhodes. 2008. Nucleosome repeat length and linker histone stoichiometry determine chromatin fiber structure. *Proc.Natl.Acad.Sci.U.S.A.* 105:8872-8877.
31. Schalch, T., S. Duda, D. F. Sargent, and T. J. Richmond. 2005. X-ray structure of a tetranucleosome and its implications for the chromatin fibre. *Nature* 436:138-141.
32. Bloomfield, V. A. 1997. DNA condensation by multivalent cations. *Biopolymers* 44:269-282.
33. Korolev, N., N. V. Berezhnoy, K. D. Eom, J. P. Tam, and L. Nordenskiöld. 2009. A universal description for the experimental behavior of salt-(in)dependent oligocation-induced DNA condensation. *Nucleic Acids Res.* 37:7137–7150.